

ORIGINAL ARTICLE

Design and Clinical Evaluation of a Handheld Wavefront Autorefractor

Nicholas J. Durr*, Shivang R. Dave*, Fuensanta A. Vera-Diaz†, Daryl Lim*, Carlos Dorronsoro*, Susana Marcos*, Frank Thorn†, and Eduardo Lage*

ABSTRACT

Purpose. To introduce a novel autorefractor design that is intended to be manufacturable at low cost and evaluate its performance in measuring refractive errors.

Methods. We developed a handheld, open-view autorefractor (the “QuickSee” [QS]) that uses a simplified approach to wavefront sensing that forgoes moving parts and expensive components. Adult subjects ($n = 41$) were recruited to undergo noncycloplegic refraction with three methods: (1) a QS prototype, (2) a Grand Seiko WR-5100K (GS) autorefractor, and (3) subjective refraction (SR). Agreements between the QS and GS were evaluated using a Bland-Altman analysis. The accuracy of both autorefractors was evaluated using SR as the clinical gold standard.

Results. The spherical equivalent powers measured from both autorefractors correlate well with SR, with identical correlation coefficients of $r = 0.97$. Both autorefractors also agree well with each other, with a spherical equivalent power 95% confidence interval of ± 0.84 diopters (D). The difference between the accuracy of each objective device is not statistically significant for any component of the power vector ($p = 0.55, 0.41, \text{ and } 0.18$, for $M, J_0, \text{ and } J_{45}$, respectively). The spherical and cylindrical powers measured by the GS agree within 0.25 D of the SR in 49 and 82% of the eyes, respectively, whereas the spherical and cylindrical powers measured by the QS agree within 0.25 D of the SR in 74 and 87% of the eyes, respectively.

Conclusions. The prototype autorefractor exhibits equivalent performance to the GS autorefractor in matching power vectors measured by SR.

(Optom Vis Sci 2015;92:1140–1147)

Key Words: refraction, wavefront aberrometry, autorefractor, refractive errors, global health

Uncorrected refractive errors are a leading cause of disability globally and are especially prevalent in low-resource settings.¹ One of the major barriers to obtaining prescription eyeglasses in these settings is that eye care is often inaccessible—there is a shortage of eye care professionals and the efficiency of existing providers is limited by a lack of equipment.² Autorefractors are used ubiquitously in high-resource settings to expedite the refraction process and enable minimally trained personnel to measure eyeglass prescriptions, but they are too expensive for widespread adoption in low-resource settings.

An eyeglass prescription contains a minimum of three numbers that characterize the refractive power of each eye (the “refraction”): the spherical power, S , cylinder power, C , and the axis, A . The six parameters (three for each eye) obtained with an autorefractor are often used as a starting point for subjective refraction (SR) and to reduce the overall time required of an examiner to obtain an eyeglass prescription. Standard autorefractors use high-quality optical components with moving parts and are traditionally large, stationary systems. Portable autorefractors such as the Nikon Retinomax are also available, but these are more expensive and less accurate than standard tabletop systems.^{3,4} There are also emerging low-cost techniques for objective refraction that use adjustable lenses^{2,5,6} or a modified mobile phone,⁷ but these approaches have yet to demonstrate comparable accuracy to commercial autorefractors or the gold standard of SR.

This study introduces and clinically evaluates a new, custom-developed, handheld autorefractor called the QuickSee (QS). It is based on Shack-Hartmann wavefront sensing, but unlike

*PhD

†OD, PhD

Madrid-MIT M+Visión Consortium, Massachusetts Institute of Technology, Cambridge, Massachusetts (NJD, SRD, DL, EL); Department of Biomedical Engineering, Johns Hopkins University, Baltimore, Maryland (NJD); New England College of Optometry, Boston, Massachusetts (FAV-D, FT); Instituto de Óptica “Daza de Valdés,” Consejo Superior de Investigaciones Científicas, Madrid, Spain (CD, SM); and Instituto de Investigaciones Biomédicas “Alberto Sols,” UAM/CSIC, Madrid, Spain (EL).

conventional wavefront aberrometers, the QS is composed of low-cost components, a simplified optical layout, and no moving parts. The prototype is also open view, which reduces the influence of instrument-induced myopia. Refractions obtained from the QS prototype were compared with those obtained with a Grand Seiko WR-5100K (GS) open-view autorefractor and with binocular SR. The GS autorefractor model chosen for comparison in this study is frequently used in other clinical studies and known to agree well with SR.^{8,9}

METHODS

QS Prototype

The QS prototype tested in this study is a new, simplified implementation of a Shack-Hartmann wavefront aberrometer. It differs from conventional wavefront aberrometers in a number of ways: (1) it uses a laser diode as a light source instead of a superluminescent diode, (2) it uses a low-cost complementary metal-oxide-semiconductor detector instead of a scientific-grade charge-coupled device for the wavefront sensor, (3) there is no Badal relay lens system in either the illumination or detection paths, (4) there is no dedicated pupil camera, and (5) it is a see-through device. These modifications allow for a simplified layout (Fig. 1A); a compact, handheld form factor (Fig. 1B); and a reduced bill of materials. Much of the reduction in performance that would result from the removal and reduction in quality of components compared with a conventional wavefront aberrometer is mitigated with the use of a custom data processing algorithm that examines many recorded wavefront images to calculate the refractive power of the eye.

The removal of the Badal system in our aberrometer does create three complications that have the effect of reducing the measurement range, but not significantly reducing performance within the measurement range. First, the illumination beam is always collimated entering the pupil, resulting in large spots on the retina for eyes with severe primary aberrations. Because the retinal plane is approximately conjugate with the image sensor plane, this can result in large spots in the Shack-Hartmann image that are difficult to

isolate. Second, without moving lenses to compensate for defocus aberration, the envelope of the wavefront may converge or diverge as it enters the microlens array (Fig. 1A, inset). Thus, for severe myopia, the wavefront will be undersampled by the lenslet array, and for severe hyperopia, the periphery of the pupil is not sampled. Third, because the pupil plane is not optically conjugate with the microlens array in our configuration, the refraction calculated at the microlens array must be propagated to the spectacle plane using a vertex correction.

The QS prototype uses an 850-nm laser diode that delivers an average power to the eye of 250 μW with a beam diameter, D_b , of 1 mm at the cornea. The safety threshold for viewing 850-nm collimated light for 5 minutes continuously is 332 μW , as specified by the ANSI Z136.1-2000 Standard for protection of the human eye.¹⁰ The laser diode creates a point on the retina of the subject, the light from which is then remitted through the pupil, passed through an 850-nm band-pass filter with a 10-nm full width at half maximum, and analyzed with a custom wavefront sensor. The choice of a relatively high power source enabled a high signal-to-noise ratio of the spots in the Shack-Hartmann image at fast imaging rates. This proved to be especially important in patients with strong refractive errors where the beacon generated on the retina is blurred. Additionally, a bright source facilitated alignment of the prototype for the subject. We also include a 1.0 neutral density filter at the output port of the prototype that attenuates the ambient light in the see-through channel to increase the contrast of the source for the subject.

The propagation distance from the pupil to the lenslet array, l_1 , is 105 mm. The wavefront sensor is composed of a 1.2-mm-thick, 10- \times 10-mm microlens array and a 1.3-megapixel monochrome complementary metal-oxide-semiconductor image sensor with a 5.3- \times 6.7-mm active area. Each lens in the microlens array is plano on one side and convex parabolic on the other side with a focal length, f_l , of 19 mm and a pitch, p , of 300 μm . The QS prototype connects to an external power source and a laptop computer that records and processes wavefront images.

Eye refractions are calculated automatically, with no human intervention, using a custom algorithm that analyzes the sequence

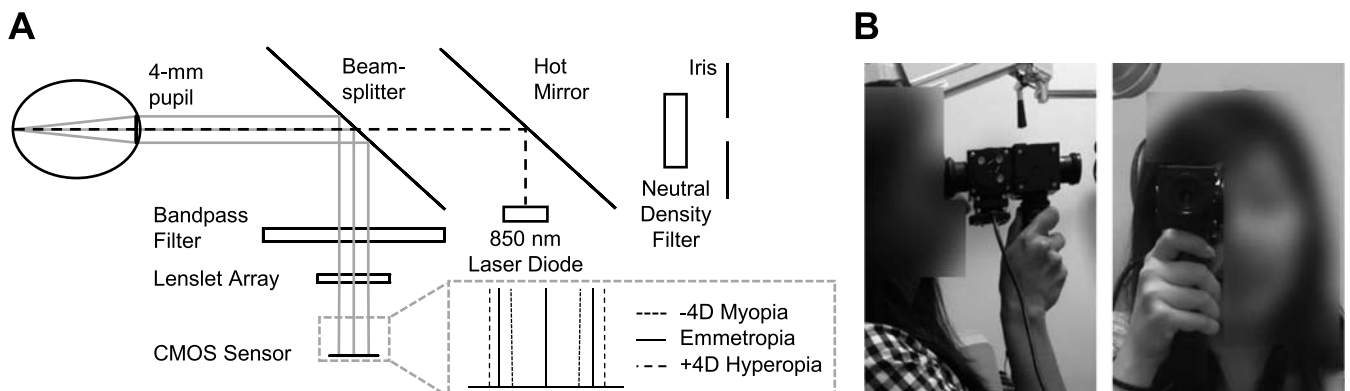


FIGURE 1.

(A) Layout of the QS low-cost open-view autorefractor. An 850-nm laser diode illuminates a point on the retina (dashed red line) and a custom-built wavefront sensor captures the remitted light field (solid blue lines). This schematic shows the wavefront envelope simulated with Zemax from a 4-mm-diameter pupil of an emmetropic eye. The inset shows a magnified view of the wavefront envelope from eyes that are -4 D myopic, $+4$ D hyperopic, and emmetropic. The width of the image sensor (6.66 mm) shows the size of the wavefront envelope relative to the size of the sensor. (B) Photographs of the QS in use show that the layout can be implemented in a compact prototype that can be held and aligned by the subject. A color version of this figure is available online at www.optvissci.com.

of wavefront images recorded by the QS. To optimize the exposure of the recorded wavefront images, a closed-loop control system adjusts the frame rate (from 5 to 25 Hz) and exposure time (from 40 to 200 ms) of the detector to maintain a target percentage (0.1%) of saturated pixels in the image. After the video acquisition is complete, the algorithm removes unusable frames from the raw image sequence using a set of quality metrics. The most common causes for unusable frames in the 41 patients tested here were (1) misalignments between the eye and the device, (2) low signal owing to saturated pixels from corneal reflections, and (3) no signal attributed to the subject blinking. Frames are also removed if they contain less than 21 resolvable spots, which is the minimum required for fitting a sixth-order Zernike polynomial. An average of 281 ± 113 frames was recorded per video. After removing unusable frames, there was an average of 137 ± 93 wavefront images remaining to analyze in each video. The input data to the QS algorithm are thus substantially different from conventional wavefront aberrometers, which typically calculate aberrations from a single frame rather than from a dynamic sequence of wavefront images.

Wavefront images that pass the filtering stage are evaluated individually to create a set of refractions and then the statistics of the set are analyzed to generate the final prescription. Depending on the number of spots identified in the image, the slopes of the wavefront sampled within each lenslet are fitted to a 6th- to 10th-order Zernike polynomial expansion using least-squares estimation.¹¹ The second-order Zernike coefficients are used to determine the power vector representation of the refraction (M , Jackson cross-cylinder components at 0 degrees, J_0 , and at 45 degrees, J_{45}),¹² using well-known formulas.¹³ The magnitudes of some higher-order coefficients are known to correlate with visual acuity,¹⁴ but we found that evaluating only the low-order aberrations resulted in accurate autorefractive. The software groups the refractions in sets with similar M , J_0 , and J_{45} (binned at 0.125-diopter [D] increments), and the average value in the data set with the largest number of elements (the statistical mode of the histogram) is used as the uncalibrated refraction value.

The QS is calibrated by measuring refractions from an emmetropic model eye with known trial lenses placed at the spectacle plane to vary M , J_0 , and J_{45} , independently. The model eye has a 5-mm-diameter iris in front of a 19-mm-focal-length doublet lens (Thorlabs AC127-019-B-ML) with a flat surface placed approximately at a focal distance behind the lens to act as the retina. Values from these uncalibrated measurements are interpolated piecewise and applied to each power vector component measured by the QS to generate the calibrated output. In addition to this calibration, an additional offset is expected to account for the difference in dispersion between the model eye and human eye. The model eye has a defocus shift of only 0.25 D (calculated in Zemax) whereas a human eye is expected to have a defocus shift of about 0.75 D between 850 and 543 nm.¹⁵ However, in our pilot human tests, we found that we did not need to include an offset to account for the 0.5-D difference in the QS refractions to agree with the GS and SR. This discrepancy is attributed to the model eye being emmetropic at green wavelengths, which was later confirmed by a measurement of -0.5 D of myopia by a commercial autorefractor.

The myopic range of the QS is limited by ray crossover—when the wavefront converges so strongly that spots formed on the image

sensor from adjacent lenslets cannot be resolved. For a system like the QS, with no compensation optics between the eye and the lenslet array or the light source, Campbell¹⁶ has used geometric optics to derive a relation for the minimum refractive error measurable, P_{\min} :

$$P_{\min} = - \left\{ \frac{1}{2f_1} - \frac{\delta_s}{2p} \right\} / \left\{ 1 + \frac{D_b \cdot l_e}{2p \cdot l_p \cdot n} \right\} \quad (1)$$

where δ_s is the tangent of the angle subtended by the source, l_e is the distance between the retina and the second principal plane of the eye, l_p is the distance between the retina and the second nodal point of the eye, and n is the index of refraction of the eye. Using values of $\delta_s = 0.0067$, $l_e = 23$ mm, $l_p = 17$ mm, and $n = 1.336$, the theoretical P_{\min} of the QS prototype is -5.7 D. This agrees well with the measured limit of -6 D determined by measuring trial lenses with a model eye.

In hyperopic eyes, the wavefront envelope expands as it propagates from the pupil to the lenslet array. Thus, the hyperopic range of the QS, P_{\max} , is limited by the diameter of the pupil, D_p , desired to be sampled and the diameter of the wavefront sensor, D_s . The maximum measurable refractive power can then be determined by geometric optics to be:

$$P_{\max} = \frac{D_1 - D_p}{D_p \cdot l_1} \quad (2)$$

The smallest dimension measured by the QS wavefront sensor is 5.3 mm. In this model, the QS can measure up to 7 D of hyperopia while still sampling at least a 3-mm diameter of the pupil.

Experimental Protocol

Institutional review boards at both the New England College of Optometry and Massachusetts Institute of Technology approved the protocol used in this study. The study also conformed to the tenets of the Declaration of Helsinki. Subjects were recruited from the students and staff at the New England College of Optometry via e-mail requests to approximately equally populate four refractive groups categorized by their spherical equivalent power, M : high myopes ($-6.00 \text{ D} \leq M < -3.00 \text{ D}$), low myopes ($-3.00 \text{ D} \leq M < -0.50 \text{ D}$), emmetropes ($-0.50 \text{ D} \leq M < 1.00 \text{ D}$), and hyperopes ($1.00 \text{ D} \leq M < 4.00 \text{ D}$) as measured with SR. Additional criteria for inclusion were (1) no history of surgery or eye disease, (2) age between 18 and 64 years, (3) best-corrected visual acuity of 20/20 or better in each eye, (4) astigmatism of less than or equal to 3 D, and (5) not using drugs, systemic or ocular, that may affect vision. Informed consent was collected for participation in the study and, optionally, for being photographed while using the QS prototype.

Refractions were performed on both eyes of every subject without the use of cycloplegia. Subjects were first measured with a GS and then with the QS prototype. Lastly, an experienced optometrist performed binocular SR on the subject, using the GS measurement as a starting point. We note that starting from the GS measurement may bias the SR from the optometrist, resulting in a worst-case comparison of the accuracy of the QS device in matching SR. The GS measurement was determined from an average of five measurements of the GS autorefractor set to high accuracy mode while the subjects looked at a target placed 20' away. When subjects used the QS prototype, they were instructed to hold and look

through the device at an external target placed 20' away. Subjects were asked to manually adjust the position of the device until they could see a bright red spot and then to look at the target across the room with both eyes open while a 30-second video was recorded. Three 30-second videos were recorded for each eye. The first video was considered a practice run for the subject to align the device. The analysis presented here was performed on the wavefront images recorded from the last two videos of each eye.

Analysis of Autorefractor Performance

Refractions obtained from each of the three methods were compared in both the refractive domain (S , C , and A) and the power vector domain (M , J_0 , and J_{45}). First, to evaluate the agreement between the QS and the GS measurements, we perform a Bland-Altman analysis on the independent components of the power vector measurements as well as the total dioptric strength of the combined components ($TDS = \sqrt{M^2 + J_0^2 + J_{45}^2}$).¹⁷ Second, using SR as the gold standard, we compare the errors in power vector measurements of the QS and GS autorefractors. In this case, we define the TDS error as the TDS of the difference between each component of the power vector measured by objective refraction and SR. Differences in error distributions were evaluated using a Wilcoxon signed rank test with a criterion of p less than 0.05 for statistical significance. Only the results from the right eye for each subject were considered in the statistical test to avoid the influence of isometropia on the independence of the samples. Third, we compare the agreement between the refractions provided by both autorefractors and SR within thresholds of 0.25 and 0.50 D of optical power and 10 and 20 degrees of cylindrical orientation. The axis agreement is calculated by only evaluating eyes that have a nonzero cylinder measurement by SR ($|C| \geq 0.25$ D).

RESULTS

We tested the accuracy and variability of the QS calibration by applying the calibration to a test set of three new measurements of each trial lens used for the calibration. Uncalibrated measurements tended to slightly underestimate the magnitude of power of the trial lens for each power vector component except in eyes with greater than 8 D of hyperopia (Fig. 2). Because the model eyes we tested have a relatively constant power with smaller apertures, we were able to measure the correct power of tested trial lenses to over 10 D of hyperopia. The calibrated measurements demonstrated excellent agreement with the power of the tested trial lenses. In the linear regime of the spherical equivalent power measurements (-1 to $+1$ D), the calibration has an average offset of 0.32 D.

Forty-three subjects were enrolled in the study, but two were determined to be outside of the M range for inclusion during the procedure (both were more than -6 D M myopic). Both subjects were removed from the analysis. The remaining 41 patients (32 were female), ranged in age from 21 to 62 years (26.4 ± 9.7 years). There were no observed adverse events in this study and we were able to obtain refractions for all recruited subjects using each of the three refraction methods.

Comparing the power vectors measured from the QS and the GS with a Bland-Altman analysis, we find average differences of -0.19 , -0.20 , 0.09 , and 0.06 D for M , J_0 , J_{45} , and TDS ,

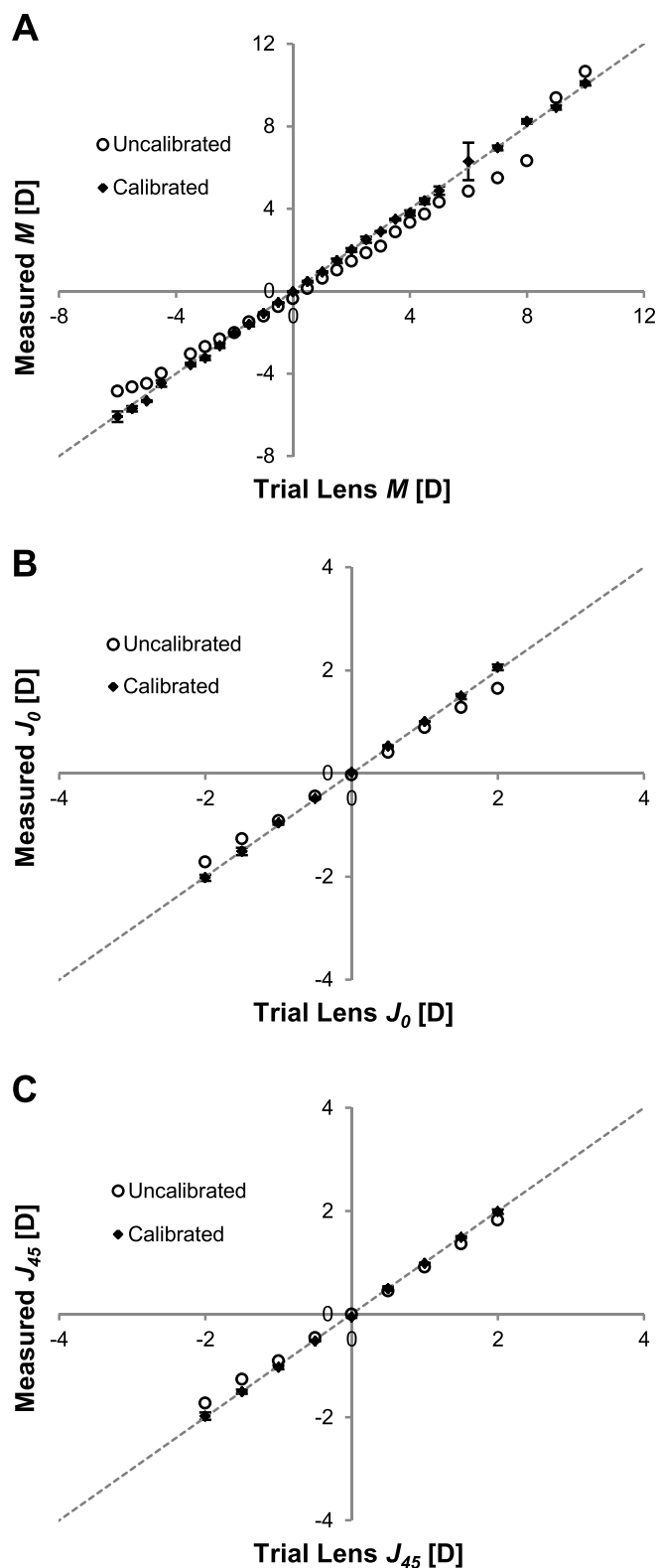


FIGURE 2.

QuickSee calibration and test measurements of trial lens combinations that independently vary the spherical equivalent power, M (A), the vertical Jackson cross-cylinder power, J_0 (B), and the oblique Jackson cross-cylinder power, J_{45} (C). The uncalibrated measurements indicate the output of the QS algorithm using an analytical calculation. These measurements are interpolated piecewise and used to calibrate QS measurements. Calibrated points show the mean and SD of a set of three separate measurements of each trial lens combination.

respectively, with the QS providing lower mean values of M and J_0 and higher average values of J_{45} and TDS than the GS (Fig. 3). The 95% confidence limits of agreement (1.96σ) between the QS and GS are ± 0.85 , ± 0.32 , ± 0.25 , and ± 0.90 D for M , J_0 , J_{45} , and TDS , respectively, although the subjects only spanned a small range of J_{45} values (-0.38 to 0.26 D when measured by the GS).

Power vector measurements are strongly correlated between the objective refraction and SR techniques (Fig. 4). The GS and SR measurements of M were correlated with a Pearson linear correlation coefficient of $r = 0.97$ ($p = 2.4 \times 10^{-51}$). The QS and SR measurements of M were correlated with a Pearson linear correlation coefficient of $r = 0.97$ ($p = 6.4 \times 10^{-53}$). The average difference between M measured by the objective and subjective technique was -0.08 D for the GS and 0.13 D for the QS. There are no significant systematic measurement differences associated with the magnitude of the refractive error. However, one young hyperopic subject was an outlier for the spherical equivalent measurements in both eyes with both objective techniques compared with the SR. This subject reported to have known difficulties when obtaining her refractive error as it fluctuates

significantly because of overaccommodation problems. She is a corrected moderate hyperope, and the SR matched her current eyeglass correction. Therefore, these values are used to compare with the objective measurements, both of which showed to be much less hyperopic.

The mean and SD of the absolute value of the errors for each autorefractor versus SR are similar (Table 1). Because the error variables are not normally distributed, we tested for statistical significance of the differences with a Wilcoxon signed rank test. There were no statistically significant differences ($p > 0.05$ in every case) in the error distribution of the power vector components measured with the QS device compared with the GS device, indicating that they have similar accuracy in the power vector domain.

To investigate systematic bias in the astigmatism measured by each autorefractor compared with SR, we constructed double-angle plots of the cross-cylinder difference vectors. Fig. 5 shows that both the QS and the GS autorefractor had asymmetrical spreads, with the QS exhibiting a center of distribution of 0.12 D at 161 degrees and the GS exhibiting a center of distribution of 0.10 D at 84 degrees. We also investigate the error rates of each

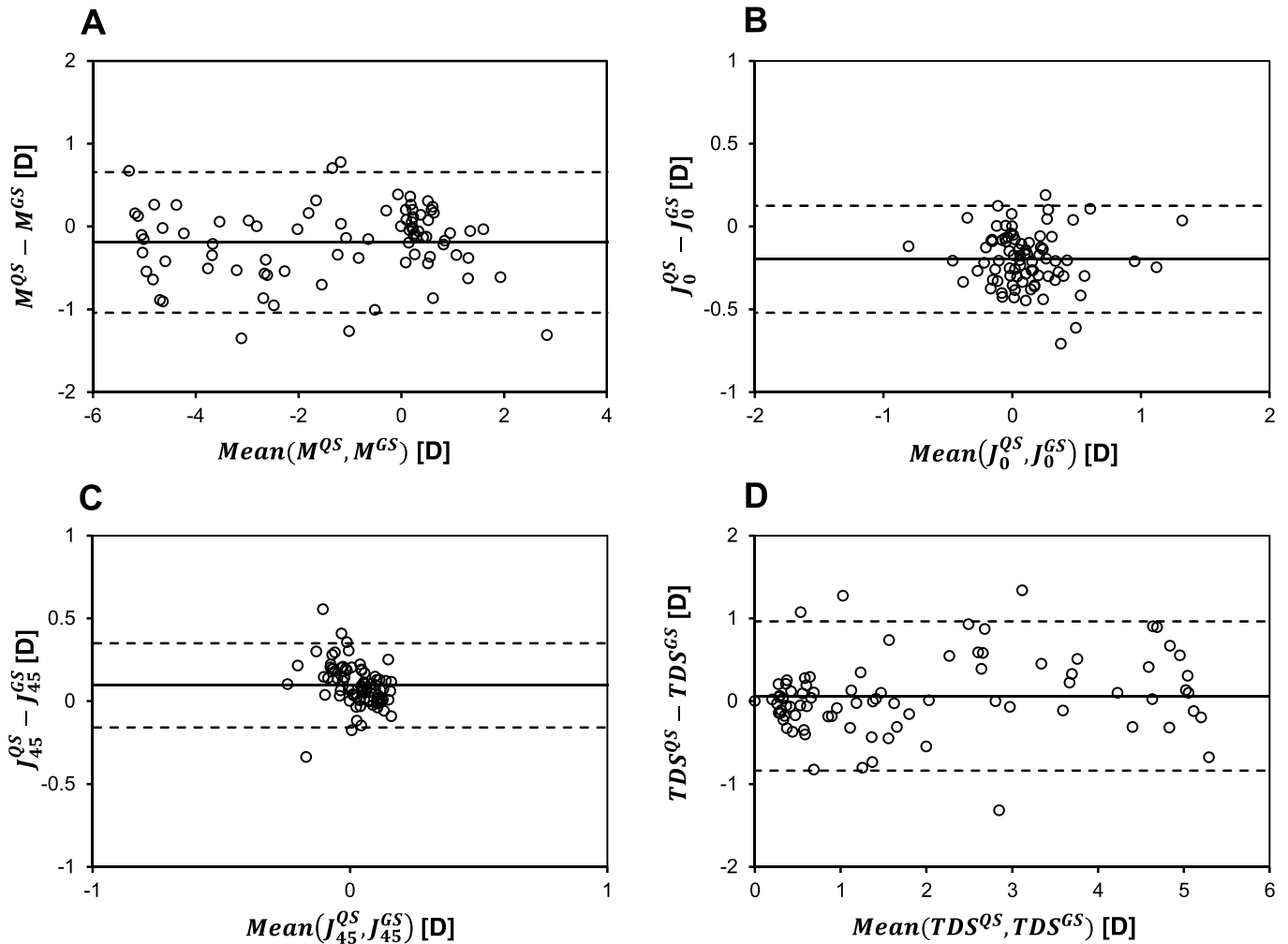


FIGURE 3. Bland-Altman plots show the agreement between the QS and GS autorefractors when measuring M (A), J_0 (B), J_{45} (C), and TDS (D). Solid lines represent the bias between autorefractors (mean of the measurement difference) and dashed lines are placed at the $\pm 95\%$ confidence interval for the difference. The two autorefractors agree within (mean difference $\pm 95\%$ confidence interval) -0.20 ± 0.84 D, -0.15 ± 0.31 D, 0.06 ± 0.25 D, and 0.08 ± 0.89 D, for M , J_0 , J_{45} , and TDS , respectively.

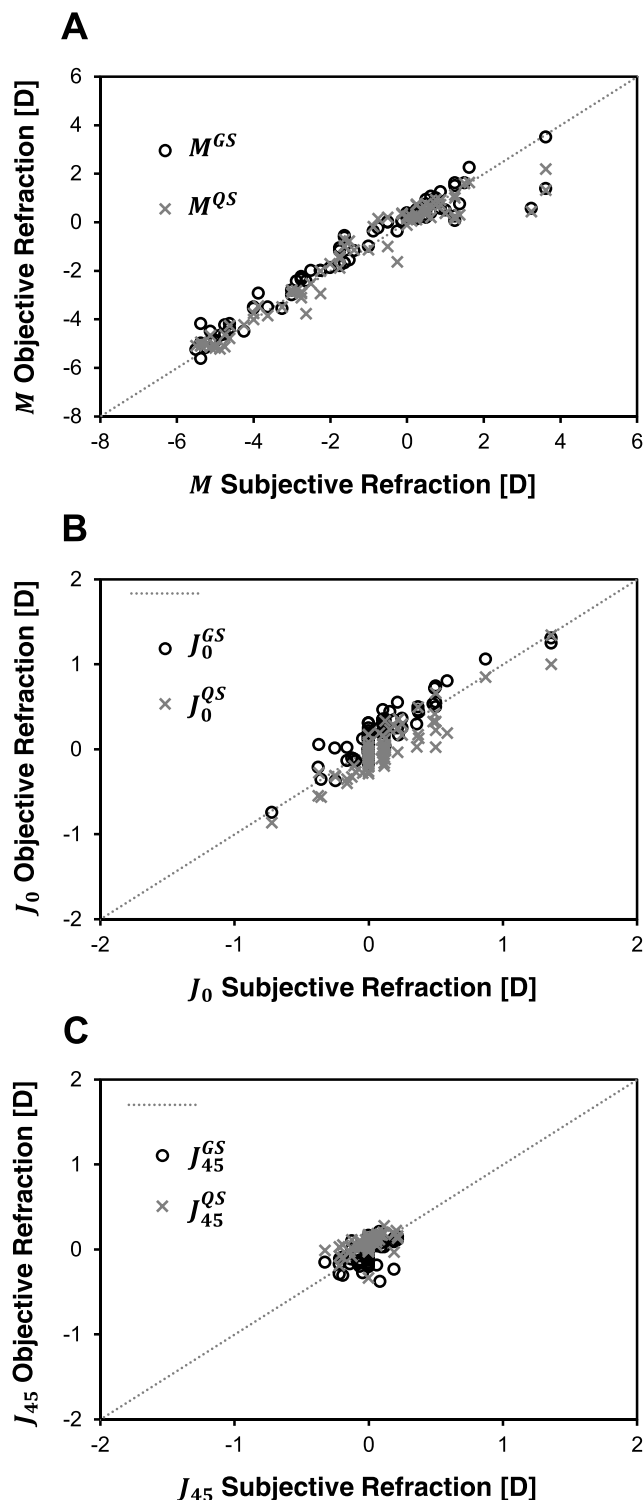


FIGURE 4.

The M (A), J_0 (B), and J_{45} (C) measured with both the GS and QS autorefractors correlate well with the SR measurements. The two hyperopic outliers in the M measurement come from two eyes of the same subject.

autorefractor in comparison to the SR results in the refractive domain. The QS provides spherical and cylindrical powers that more frequently agreed with the measurements from SR (Table 2). The QS agrees within 0.25 D of the SR S and C for 74 and 87% of the eyes, respectively, whereas the GS agrees within 0.25 D of the SR S and C for 49 and 82% of the eyes. For larger thresholds, the

performance of the QS and GS is more similar, as both devices have a similar fraction of outliers that deviated from the SR. The axis measured by the QS and GS were within 10 degrees of SR for 52 and 64% of the eyes, respectively. The poorer performance of the QS for the axis is likely attributed to variations in how the subjects held the QS prototype—the axis measurement is provided relative to the orientation of the device and most subjects did not hold the device consistently vertically.

DISCUSSION

This study evaluates the accuracy of a potentially low-cost, open-view autorefractor compared with a commonly used commercial autorefractor. One challenge in evaluating the clinical accuracy of any autorefractor is that although SR is the most relevant gold standard, it is a relatively imprecise technique that can be confounded by variations in subject feedback, as well as by uncertainties in the working distance, vertex correction distance, depth of field, and trial lens power.¹⁸ Nevertheless, previous studies have shown that SR is repeatable within 0.25 D about 80% of the time,^{18,19} and introducing as small as a 0.25-D refractive error is known to cause some discomfort to subjects.²⁰ Therefore, 0.25 D is a relevant benchmark level of accuracy to attempt to achieve in autorefractor.

The QS and GS autorefractors tested in this study measured values of M that agreed within 0.25 D of the value measured from SR in 71% and 63% of the measured eyes, respectively. This result is within the range found in other recent studies of commercial autorefractors, which have shown an agreement of M within 0.25 D of SR in 44%,^{8,21} 51%,⁸ and 57%²² of the measured eyes. There are several emerging low-cost and portable technologies currently being pursued to improve refraction in low-resource settings.² Adjustable lenses can be used for self-refraction and can be locked to provide the prescription eyeglasses after refraction. However, at present, they either only correct for defocus errors or, in one case, require the subject to go through a challenging three-parameter optimization process to tune S , C , and A for each eye.^{2,5,6} Another approach is to retrofit a mobile phone to act as an adjustable Scheiner disk.⁷ This strategy has the advantage of being low cost if a mobile phone with a high-quality screen is already available.

TABLE 1.

Power vector measurement errors of the GS and QS autorefractors

Power vector	Objective test	Mean \pm SD of absolute error of right eyes, D	p
M	GS	0.40 \pm 0.46	0.55
	QS	0.41 \pm 0.53	
J_0	GS	0.14 \pm 0.10	0.41
	QS	0.16 \pm 0.11	
J_{45}	GS	0.09 \pm 0.08	0.18
	QS	0.10 \pm 0.06	
TDS	GS	0.47 \pm 0.44	0.55
	QS	0.49 \pm 0.51	

Errors are calculated using SR as the gold standard. We found that there is no statistically significant difference (a p value of >0.05 for each power vector component) between the accuracies of the two autorefractors in measuring power vectors.

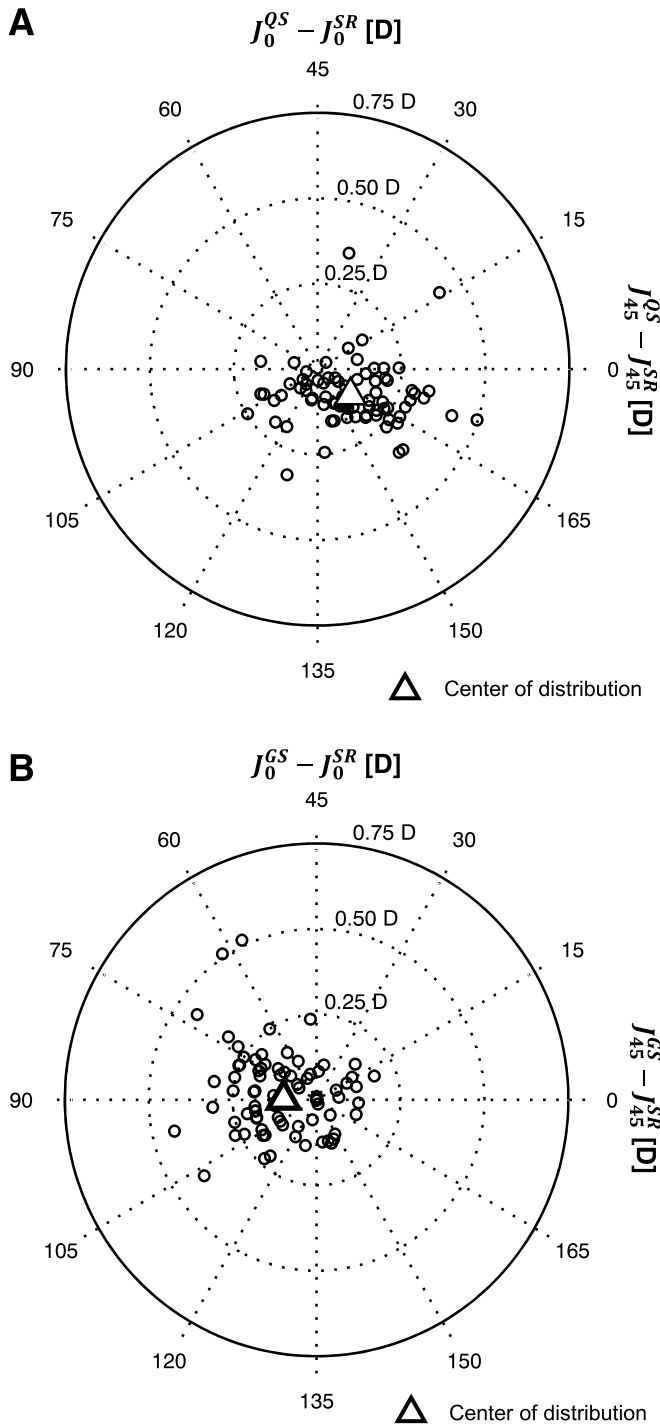


FIGURE 5. Double-angle astigmatic distribution of the cross-cylinder difference vectors between the QS and SR (A) and the GS and SR (B). The centers of the distributions are located at 0.12 D at 161 degrees and 0.10 D at 84 degrees from the origin for the QS and GS measurements, respectively. All measurements fell within a 0.50-D-radius circle except for two eyes measured with the GS autorefractor.

However, in a recent study on 34 eyes, the *M* measured with the mobile phone refractometer was found to agree within 0.25 D of the SR in only 15% of the measured eyes.²³

There are several areas in which the QS could be improved. The range of the current prototype is limited to subjects with an *M* of greater than or equal to -6.0 D of myopia. With this range, an

autorefractor can provide a prescription to about 95% of adults, depending on the population.^{24,25} To cover a larger portion of the population, the range must be expanded to work for patients with more severe myopia. Additionally, the usability and speed of the QS could be improved to make alignment easier for the patient and to reduce the measurement time from 60 seconds (two 30-second videos) closer to the approximately 10 seconds that the commercial autorefractors take. These usability and speed constraints are related to each other in that as the prototype is made more intuitive and robust to alignment errors, the time required to record a sufficient number of high-quality wavefront images will be reduced. Improvements in usability and speed will also facilitate the testing of this device in a more diverse population, including children and elderly patients.

The accuracy of the QS could also be improved. We found an average spherical equivalent power error of 0.12 D, which is likely attributed to chromatic defocus. After testing a larger number of eyes, this offset can be incorporated into the calibration, and this systematic error can be reduced. The axis measurement from the QS was likely limited by the handheld use of the device. Subjects were instructed to hold the device with the handle vertically but would often tilt the prototype relative to their face. This limitation may be overcome by incorporating a contralateral viewing channel for the opposite eye (a binocular port) so that the axis of the device is fixed relative to the axis between the two eyes of each subject. There is also the potential to increase the accuracy of the prototype by incorporating more sophisticated algorithms that analyze the higher-order aberrations measured by the device.^{13,26}

To make further progress toward a low-cost autorefractor, several additional steps are necessary to replace the remaining high-cost components of the prototype evaluated here: (1) a low-cost microcontroller and display should be incorporated into the device to replace the laptop currently needed for operation, (2) the 10- × 10-mm lenslet array currently used overfills the image sensor and should be replaced with a smaller clear-aperture lenslet array, and (3)

TABLE 2.

Agreement between refractive parameters measured by objective refraction and SR

Refractive parameter	Objective test	Agreement with SR	
		≤0.25 D:	≤0.5 D:
S	GS	49%	80%
	QS	74%	82%
C	GS	82%	98%
	QS	87%	95%
A	GS	≤10 degrees: 64%	≤20 degrees: 85%
	QS	≤10 degrees: 52%	≤20 degrees: 82%
M	GS	≤0.25 D: 63%	≤0.5 D: 89%
	QS	≤0.25 D: 71%	≤0.5 D: 82%

The frequency of agreement was calculated for absolute difference thresholds of 0.25 and 0.5 D for power measurements and 10 and 20 degrees for axis measurements. The axis accuracy is reported from only the set of eyes that had a nonzero cylinder power ($|C| \geq 0.25$ D) measured by SR. The GS and QS autorefractors measured a spherical equivalent power that was within 0.25 D of the SR measurement for 63% and 71% of the measured eyes, respectively.

a custom, monolithic housing should be designed to house and orient the prototype parts.

CONCLUSIONS

This study introduces a novel wavefront-sensing autorefractor and demonstrates that it is as accurate as a high-end commercial autorefractor in predicting the power vectors measured by SR in a population of adults with a moderate range of refractive errors (−6 D of myopia to +4 D of hyperopia). Given that this autorefractor was implemented in a compact prototype using low-cost components and no moving parts, it is an encouraging step toward the development of an autorefractor that is portable, affordable, and robust.

ACKNOWLEDGMENTS

This work has been financially supported by the Comunidad de Madrid through the Madrid-MIT M+Visión Consortium. We thank the M+Visión IDEA³ faculty panel for their assistance in developing this project. We also thank the subjects who participated in the clinical testing of the QuickSee.

NJD, SRD, DL, CD, SM, and EL are inventors on patents relating to the autorefractor used in this study and have a financial interest in PlenOptika, Inc. Since the completion of the study NJD, SRD, DL, and EL have become part-time employees of PlenOptika.

Received January 21, 2105; accepted July 10, 2015.

REFERENCES

- Resnikoff S, Pascolini D, Mariotti SP, Pokharel GP. Global magnitude of visual impairment caused by uncorrected refractive errors in 2004. *Bull World Health Organ* 2008;86:63–70.
- Durr NJ, Dave SR, Lage E, Marcos S, Thorn F, Lim D. From unseen to seen: tackling the global burden of uncorrected refractive errors. *Annu Rev Biomed Eng* 2014;16:131–53.
- Farook M, Venkatramani J, Gazzard G, Cheng A, Tan D, Saw SM. Comparisons of the handheld autorefractor, table-mounted autorefractor, and subjective refraction in Singapore adults. *Optom Vis Sci* 2005;82:1066–70.
- Choong YF, Chen AH, Goh PP. A comparison of autorefraction and subjective refraction with and without cycloplegia in primary school children. *Am J Ophthalmol* 2006;142:68–74.
- Douali MG, Silver JD. Self-optimised vision correction with adaptive spectacle lenses in developing countries. *Ophthalmic Physiol Opt* 2004;24:234–41.
- Barbero S, Rubinstein J. Power-adjustable sphero-cylindrical refractor comprising two lenses. *Opt Eng* 2013;52:63002.
- Pamplona VF, Mohan A, Oliveira MM, Raskar R. NETRA: interactive display for estimating refractive errors and focal range. *ACM Trans Graphic* 2010;29:77–84.
- Davies LN, Mullen EA, Wolffsohn JS, Gilmartin B. Clinical evaluation of the Shin-Nippon NVision-K 5001/Grand Seiko WR-5100K autorefractor. *Optom Vis Sci* 2003;80:320–4.
- Cleary G, Spalton DJ, Patel PM, Lin PF, Marshall J. Diagnostic accuracy and variability of autorefraction by the Tracey Visual Function Analyzer and the Shin-Nippon NVision-K 5001 in relation to subjective refraction. *Ophthalmic Physiol Opt* 2009;29:173–81.
- Delori FC, Webb RH, Sliney DH; American National Standards Institute. Maximum permissible exposures for ocular safety (ANSI 2000), with emphasis on ophthalmic devices. *J Opt Soc Am A* 2007;24:1250–65.
- McAlinden C, McCartney M, Moore J. Mathematics of Zernike polynomials: a review. *Clin Experiment Ophthalmol* 2011;39:820–7.
- Thibos LN, Wheeler W, Horner D. Power vectors: an application of Fourier analysis to the description and statistical analysis of refractive error. *Optom Vis Sci* 1997;74:367–75.
- Thibos LN, Hong X, Bradley A, Applegate RA. Accuracy and precision of objective refraction from wavefront aberrations. *J Vis* 2004;4:329–51.
- Applegate RA, Ballentine C, Gross H, Sarver EJ, Sarver CA. Visual acuity as a function of Zernike mode and level of root mean square error. *Optom Vis Sci* 2003;80:97–105.
- Llorente L, Diaz-Santana L, Lara-Saucedo D, Marcos S. Aberrations of the human eye in visible and near infrared illumination. *Optom Vis Sci* 2003;80:26–35.
- Campbell CE. The range of local wavefront curvatures measurable with Shack-Hartmann wavefront sensors. *Clin Exp Optom* 2009;92:187–93.
- Raasch TW, Schechtman KB, Davis LJ, Zadnik K; CLEK Study Group. Collaborative Longitudinal Evaluation of Keratoconus Study. Repeatability of subjective refraction in myopic and keratoconic subjects: results of vector analysis. *Ophthalmic Physiol Opt* 2001;21:376–83.
- Smith G. Refraction and visual acuity measurements: what are their measurement uncertainties? *Clin Exp Optom* 2006;89:66–72.
- Goss DA, Grosvenor T. Reliability of refraction—a literature review. *J Am Optom Assoc* 1996;67:619–30.
- Miller AD, Kris MJ, Griffiths AC. Effect of small focal errors on vision. *Optom Vis Sci* 1997;74:521–6.
- Mullen EA, Wolffsohn JS, Gilmartin B, Tsujimura S. Clinical evaluation of the Shin-Nippon SRW-5000 autorefractor in adults. *Ophthalmic Physiol Opt* 2001;21:101–7.
- Sheppard AL, Davies LN. Clinical evaluation of the Grand Seiko Auto Ref/Keratometer WAM-5500. *Ophthalmic Physiol Opt* 2010;30:143–51.
- Bastawrous A, Leak C, Howard F, Kumar V. Validation of Near Eye Tool for Refractive Assessment (NETRA): pilot study. *J Mob Technol Med* 2012;1:6–16.
- Dandona R, Dandona L, Naduvilath TJ, Srinivas M, McCarty CA, Rao GN. Refractive errors in an urban population in Southern India: the Andhra Pradesh Eye Disease Study. *Invest Ophthalmol Vis Sci* 1999;40:2810–8.
- Vitale S, Ellwein L, Cotch MF, Ferris FL 3rd, Sperduto R. Prevalence of refractive error in the United States, 1999–2004. *Arch Ophthalmol* 2008;126:1111–9.
- Cheng X, Bradley A, Thibos LN. Predicting subjective judgment of best focus with objective image quality metrics. *J Vis* 2004;4:310–21.

Nicholas J. Durr

Johns Hopkins University

Department of Biomedical Engineering

3400 N Charles St, Clark 208D

Baltimore, MD 21218

e-mail: ndurr@jhu.edu